Supplementary Information: Novel mixed self-assembled monolayers of L-cysteine and methanol on gold surfaces under ambient conditions[†]

Vanina Gisela Franco,*[a,b] Sindy Julieth Rodríguez,[a] Florencia Carolina Calaza,[b,c] Mario César Guillermo Passeggi,[a,b] and Gustavo Daniel Ruano[d]

[a] *Instituto de Física del Litoral (IFIS Litoral), Consejo Nacional de Investigaciones Científicas y Técnicas and Universidad Nacional del Litoral (CONICET-UNL), Güemes 3450, (3000) Santa Fe, Argentina. E-mail: vanina.franco@ifis.santafe-conicet.gov.ar*

[b] *Facultad de Ingeniería Química (FIQ), Universidad Nacional del Litoral (UNL), Santiago del Estero 2829, (3000) Santa Fe, Argentina.*

[c] *Instituto de Desarrollo Tecnológico para la Industria Química (INTEC), Consejo Nacional de Investigaciones Científicas y Técnicas and Universidad Nacional del Litoral (CONICET-UNL), Güemes 3450, (3000), Santa Fe, Argentina.*

[d] *Centro Atómico Bariloche (CAB), Comisión Nacional de Energía Atómica (CNEA), Av. Exequiel Bustillo 9500, (8400) San Carlos de Bariloche, Argentina.*

1. STM CHARACTERIZATION

A. Au(100) clean surfaces

Fig. S1, reports the characterization study of a clean surface of Au(100) single-crystal substrate, surface obtained after performing a cyclic annealing process with butane flame. Fig. S1(a), shows a topography STM image (100 nm × 100 nm) of the resulting Au(100) surface acquired in the constant current mode. The image shows a stepped surface where a series of terraces devoid of prominent features are bounded by monoatomic steps. In Fig. S1(b), a profile of apparent heights acquired over a step is depicted, i.e. obtained along the straight blue line shown in image S1(a). The profile shows a height difference of 0.22 nm, measured between the average heights of the lower and upper side terraces, marked with dotted lines in the figure. This value is in good agreement with those reported in the literature, where the height of a monoatomic step informed both theoretical and experimentally for Au(100) single-crystal surfaces is 0.205 nm and 0.200 nm [1–3], respectively. Fig. S1(c), shows an enlarged topography STM image of the substrate surface, acquired on a terrace of image S1(a), where the

surface atomic structure is observed. However, in order to enhance it to determine the geometry of the atomic lattice, as well as the nearest neighbour distances, a 2D-FFT low-pass filter was applied to image S1(c), obtaining the one shown in Fig. S1(d). A height threshold was applied to this last one (image S1(d)) obtaining the image shown in Fig. S1(e). From these images, the (1×1) reconstruction is clearly distinguished on the surface [4, 5] and the distance to first neighbours between Au atoms can be measured obtaining a value of 0.28 nm as reported previously [6].
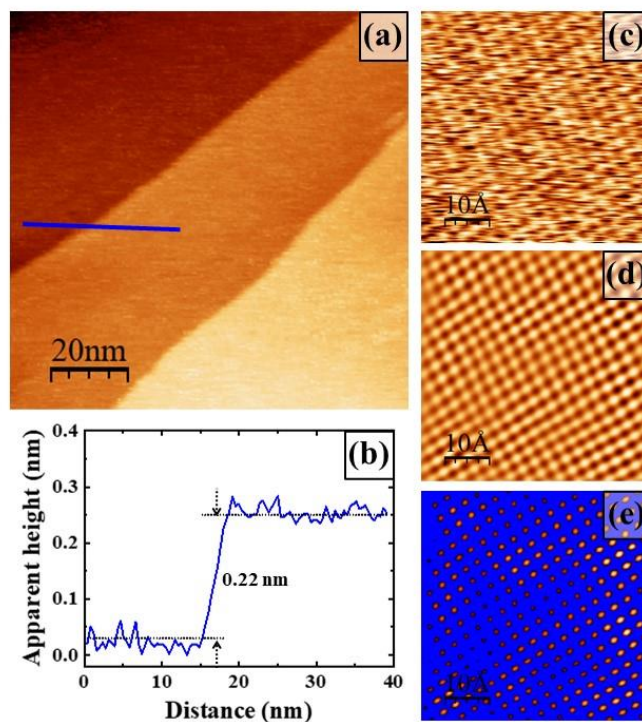
Fig. S1. (a) Topography STM image (100 nm × 100 nm) of a clean Au(100) single-crystal sur-face. (b) Apparent height profile plotted along the blue straight line depicted in image (a). (c) Detail topography STM image (5 nm × 5 nm) showing atomic resolution of the same surface shown in image (a). (d) 2D-FFT filtered image obtained from image (c). (e) Height threshold filtered image applied the image (d). Acquisition conditions: (a) V_S = +0.10 V and I_T = 0.3 nA; (c) V_S = -0.002 V and I_T = 16.0 nA.

The Au(100) samples prepared in UHV, by traditional cleaning methods [7], and in the *in- situ* measurements [4], exhibit surfaces with the well-known hexagonal reconstruction, usually referred as *hex*. This reconstruction shows rows with heights of 0.06 nm, equally spaced by a distance of 1.45 nm. [7–9]. In general, this is not the case for surfaces prepared under conditions as those in this work, which mostly show a (1×1) reconstruction [5], i.e. with surface atoms arranged in the same square structure as the underlying ones, as shown in Fig. S1(c), S1(d) and S1(e). However, the existence of the *hex* reconstruction, immediately after its preparation, can not be ruled out.

B. L-Cys SAMs on gold surfaces

Fig. S2 shows topography STM images of Au(100) and Au(111) surfaces after a 10 minutes incubation in a 10 mM L-Cys methanolic solution.
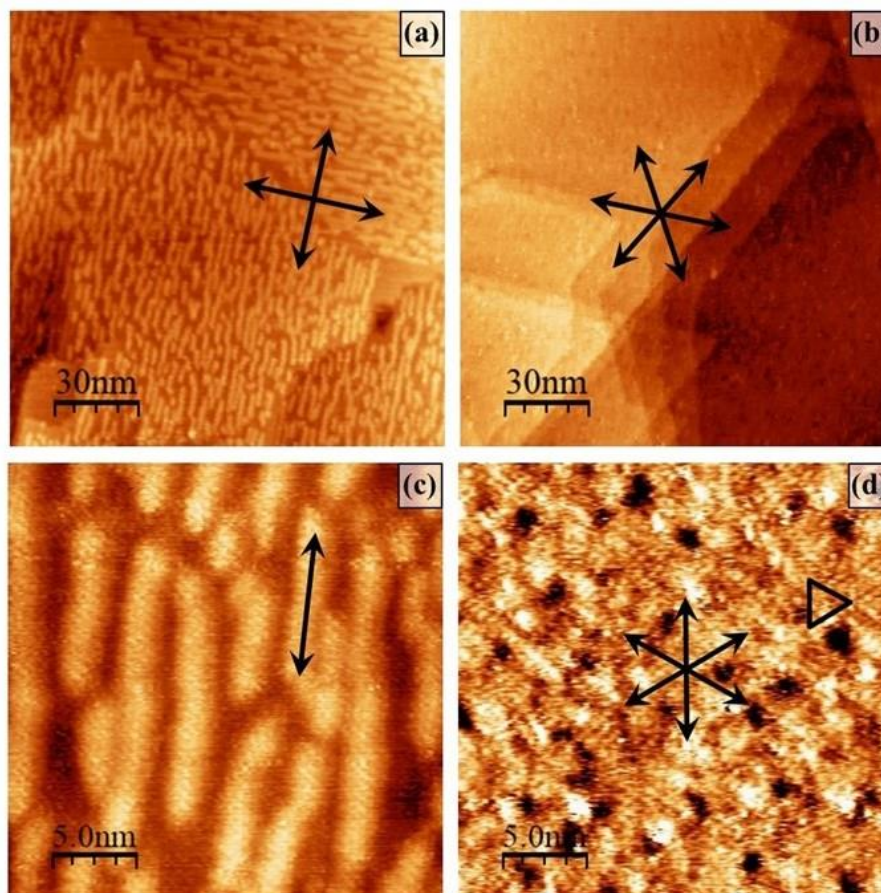
Fig. S2. Topography STM images. (a) and (b) (150 nm × 150 nm); (c) and (d) (25 nm × 25 nm). (a) and (c) are of the surface of a Au(100) single-crystal substrate incubated in a L-Cys methanolic solution. (b) and (d) are of the surface of a Au(111) single-crystal substrate incubated in a L-Cys methanolic solution. Acquisition conditions: (a) V_S = -0.78 V and I_T = 6.6 nA; (b) V_S = -0.12 V and I_T = 1.3 nA; (c) V_S = -0.78 V and I_T = 6.6 nA; (d) V_S = -0.60 V and I_T = 6.7 nA.

Fig. S2(a) show FL adsorbates, whose longitudinal axes form an angle of 90º to each other. This feature is compatible with a growth of the SAM along the high-symmetry compact directions <110> of the single crystal. It is interesting to note that domains can be delimited by 2D twinning planes being on the same terrace. Figure S2(b) shows the surface of Au(111) with a homogeneous coating after immersion in methanolic L-Cys solution. Directions of high symmetry can be seen. In Fig. S2(c), which is a higher resolution image, the arrangement of the FL structures along one of the high symmetry directions is clearly observed. In Fig. S2(d), the increase in resolution allows us to appreciate the distribution of the molecules along the three directions of high symmetry with a very low range ordering, only in some regions of the surface.

C. Procedure to find the width value of the FL structures

Through an example, Fig. S3 shows the procedure performed with a set of images, all measured with the same bias voltage to find the width of the FL structures. The width data extracted by applying an analysis to each individual image, were later combined from the uncertainty propagation of each measurement into a single width value.

Fig. S3(a) shows the matrix associated to the measured STM image, in which rows and columns are lateral pixels in the x and y directions, and the element value, i. e. the height (h) in z, is depicted in a grey scale. Each matrix was interpolated from the original STM image, to then 'rotate' it with the purpose of aligning the finger axes with the horizontal direction (along the rows of the matrix). In doing so, each column becomes a vector containing a line profile perpendicular to the FL structures.
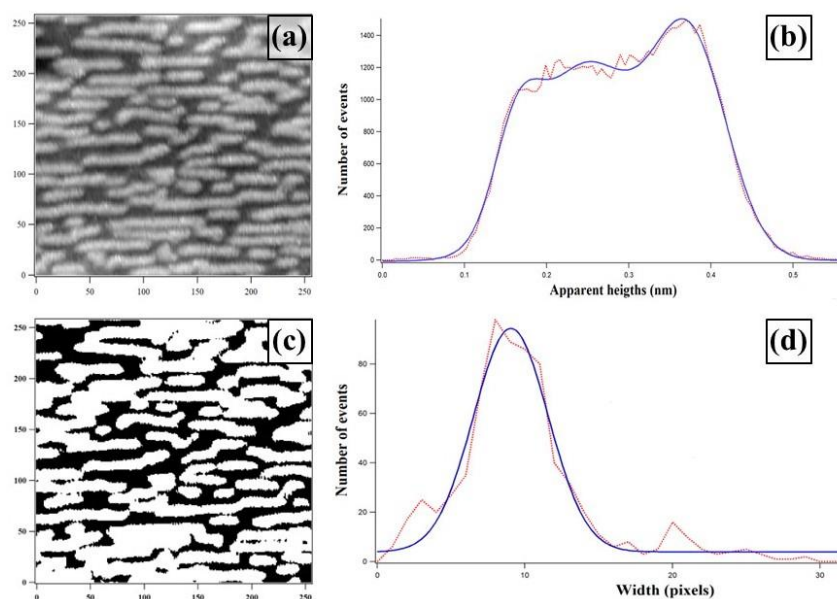
Fig. S3. (a) Dot matrix obtained from a topography STM image (252 pixels × 252 pixels) of the FL structures assembled on the surface of a Au(100) single-crystal substrate incubated during 10 minutes in a 10 mM methanol solution of L-Cys. Acquisition conditions: V_S = -0.78 V and I_T = 6.0 nA. (b) Apparent heights histogram obtained from image (a), red dot line in blue line Gaussian fitting of the histogram. (c) Discretized matrix obtained filtering matrix in (a) with a threshold resulting of averaging the peaking apparent heights in (b). (d) Histogram of finger widths in pixels.

To automate the measurement of the width of each finger, we need to discretize the values in the image matrix of Fig. S3(a). To do it, we adopted the mean-high difference as the threshold (t) to define whether a given height value (h) corresponds to a FL structure (h>t) or to the base plane (h<t). Fig. S3(b) show a height histogram (in red symbols) showing 2 predominant frequencies associated to the heights of the finger (higher value) and the base-plane (lower value), in calculating the mean of the maxima of these Gaussian

distributions (see the fitting bimodal distribution in blue line) we obtained the threshold (t). Figure S3c shows the discretized matrix associated to S3(a) with the values 1 (white) corresponding to a finger and 0 (black) to pixels in the base-plane. A simple code sorting the continuous 1 values in the each column vector produces the histogram in S3(d). By fitting it with a Gaussian (blue line) the mean width (maximum) along with the standard deviation (Gaussian width) of the measurement are obtained. Later on this values in pixels can be converted into distance.

2. XPS SPECTRA FITTING

Fitting of the spectra with respect to C 1s was carried out considering equal intensities of the Cα and Cβ signals as well as the combined peak area of carboxyl C (both protonated and neutral). Therefore, the experimental C 1s spectra are fitted with only a couple of components; a Voigt function accounting mostly for usual spurious carbon and another line-shape representing carbon atoms of the L-Cys molecules (dark grey and light-red shaded areas, respectively, in Fig. 5). This line-shape is conformed by adding up Voigt functions for the different binding energy shifts expected for the different chemical states of carbon atoms in the molecules.

During fitting, the BE of the Cβ component is allowed to change along with its intensity. The signal intensity for the other components is fixed according to the stoichiometry of the molecules I Cβ = Iα = (I$_{COO-}$ + I$_{COOH}$).

3. DFT STUDY

A. L-Cys molecule adsorbed on Au(100)

In this section, we theoretically study the most stable configuration for a single L-Cys molecule adsorbed on a Au(100) surface. To calculate the adsorption energy E_{cys}^{ads} (eV) and the adsorption distance d_{cys}^{ads} (nm), a set of relaxation processes were carried out. First, the initial geometry for the L-Cys molecule was obtained by optimizing the AA independent structure. Later, with the aim of eventually finding the most stable geometry of the system, the relaxed molecule was located on a Au(100) surface at

different heights (h)[1] and orientations: (I) C_β facing the Au(100) surface, (II) the amino-group (-NH$_2$) pointing toward the Au(100) surface, (III) the carboxyl-group (-COOH) pointing toward the Au(100) surface and (IV) the S atom facing the Au(100) surface. Figs. S4(a)-S4(d) show the initial configuration for systems I, II, III, IV, respectively. For each atomic arrangement, a total relaxation of the system was carried out (AA and Au atoms) and the total energy (E_{tot}) was calculated. The systems with the lowest total energy for each orientation are shown in Figs. S4(e)-S4(h).
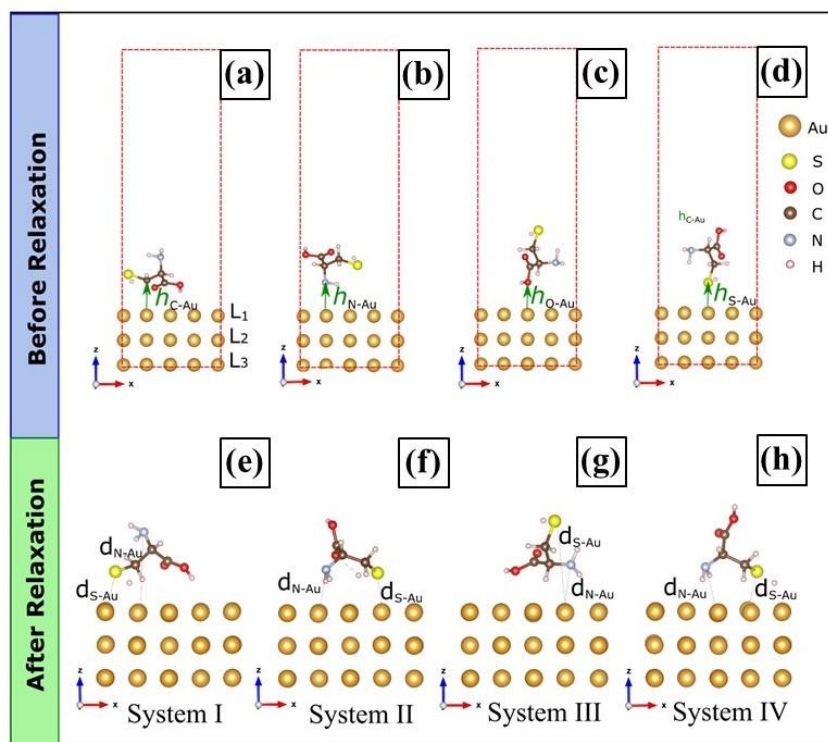
Fig. S4. Systems studied. (a) L-Cys parallel to the Au(100) surface (system I), (b) -NH$_2$ pointing towards the Au(100) surface (system II), (c) -COOH pointing towards the Au(100) surface (system III), (d) S atom facing the Au(100) surface (system IV), before relaxation. (e), (f), (g) and (h) are systems I, II, III and IV after relaxation, respectively.

The adsorption energies for the systems presented in Fig. S4 were calculated as follows:

$$E_{cys}^{ads} = E_{tot}\,(Cys/Au) - E_{tot}\,(Au) - E_{tot}\,(Cys) \tag{S1}$$

where $E_{tot}\,(Cys/Au)$ is the total energy of the L-Cys/Au system, $E_{tot}\,(Au)$ is the total energy of the Au(100) surface and $E_{tot}\,(Cys)$ is the total energy of the L-Cys molecule alone. Results of E_{cys}^{ads} and d_{cys}^{ads} for each system can be compared in Table S1. Here, a

---

[1] The heights (h) were measured between the Au surface and the C, N, O and S atoms in the initial orientations (a), (b), (c) and (d), respectively.

more negative E_{cys}^{ads} indicates spontaneous adsorption (exothermic), i.e. L-Cys tends to bind with the Au(100) surface.

Table S1. E_{cys}^{ads} and d_{cys}^{ads} for systems shown in Fig. S4. d_{cys}^{ads} is measured from the average distance of the AA to the first Au atoms layer of the Au(100) surface. d_{S-Au} and d_{N-Au} are measured from the S and N atoms towards the nearest Au atom as shown in Fig. S4.

System	E_{Cys}^{ads} (eV)	d_{Cys}^{ads} (nm)	d_{S-Au} (nm)	d_{N-Au} (nm)
I	-1.86	0.346	0.267	0.537
II	-1.59	0.357	0.256	0.325
III	-1.01	0.365	0.592	0.341
IV	-1.68	0.361	0.262	0.309

The data in Table S1 , show that the adsorption energy for the most stable system of L-Cys adsorbed on Au(100) in the gas phase is -1.86 eV (see Fig. S4(e), system I). Furthermore, the molecule does not dissociate after adsorption, so the molecular arrangement of L-Cys on the Au surface is consistent with our XPS observations, where the ratio of N and S intensities suggests that the molecule is intact. In the equilibrium configuration, the L-Cys molecule shows the -NH_2 group away from the metal surface and the S atom pointing towards the Au surface at a distance of d_{S-Au}= 0.267 nm.

B. MeOH molecule adsorbed on Au(100)

Fig. S5 presents a graphical representations of the MeOH molecules orientations on a Au(100) surface before relaxation.
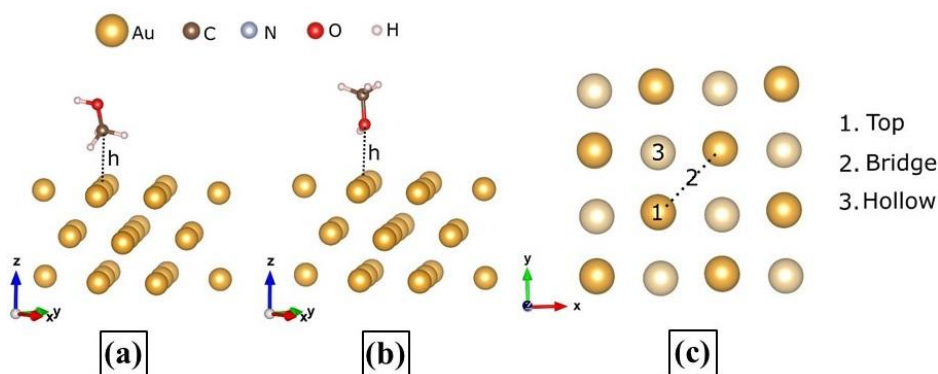
Fig. S5. Orientations of a MeOH molecule on a Au(100) surface before relaxation, (a) C and (b) O atoms pointing towards the Au(100) surface. (c) Likely adsorption sites. The Au atoms of the second layer are represented in light yellow.

The arrangements in Figs. S5(a) and S5(b) are distinguished depending on whether the carbon or oxygen atoms point towards the Au(100) surface, respectively. Fig. S5(c) shows the adsorption sites of on 1×1 Au(100) surface. In Table S2, the interaction energies of each orientation and adsorption sites for a fixed distance of 0.3 nm are reported. The interaction energy is calculated as:

$$E_{int} = E_{tot}(MeOH/Au) - E_{tot}(Au) - E_{tot}(MeOH) \qquad (S2)$$

where $E_{tot}(MeOH/Au)$ is the total energy of the MeOH molecule on the Au surface for a height of h = 0.3 nm, $E_{tot}(Au)$ is the total energy of the Au(100) surface and $E_{tot}(MeOH)$ is the total energy of the MeOH molecule alone. A comparison between the total energies of the two orientations of the MeOH molecules, allowed us to determine that the arrangement with the lowest total energy is the one in which the oxygen atom points towards the Au(100) surface, being ΔE= 18.25 meV more stable than the other configuration. Here, a more negative energy E_{int} indicates that the adsorption is spontaneous (exothermic), so according to the results, the "top" adsorption sites are less stable, since they require additional energy (endothermic). For the arrangement with the carbon atom pointing towards the Au surface, the E_{int} for the hollow site (-47.06 meV) was lower than for the top and bridge sites. On the other hand, for the arrangement with the O atom pointing towards the Au surface, the E_{int} for the hollow site (-65.32 meV) resulted lower than those for the top and bridge sites.

Table S2. E_{int} for systems shown in Figs. S5(a) and S5(b).

System	Adsorption Sites	E_{int} (meV)
	Top	+0.53
C atom pointing towards Au	Bridge	-39.89
	Hollow	-47.06
	Top	+17.47
O atom pointing towards Au	Bridge	-35.75
	Hollow	-65.32

Once it was determined that the configuration with the lowest energy occurs when the oxygen atom points toward the hollow site, a total relaxation of the molecules and the gold surface was performed for different heights h. The adsorption energy for MeOH (E_{met}^{ads}) was determined as the minimum of the interaction energy, according to the following equation:

$$E_{int}(h) = E_{tot}(MeOH/Au)(h) - E_{tot}(Au) - E_{tot}(MeOH) \qquad \text{(S3)}$$

where $E_{tot}(MeOH/Au)(h)$ is the total energy of the MeOH molecule on the Au surface for each height (h), $E_{tot}(Au)$ is the total energy of the Au(100) surface and $E_{tot}(MeOH)$ is the total energy of the MeOH molecule alone. After total relaxation, the configuration with the lowest energy is shown in Fig. S6.
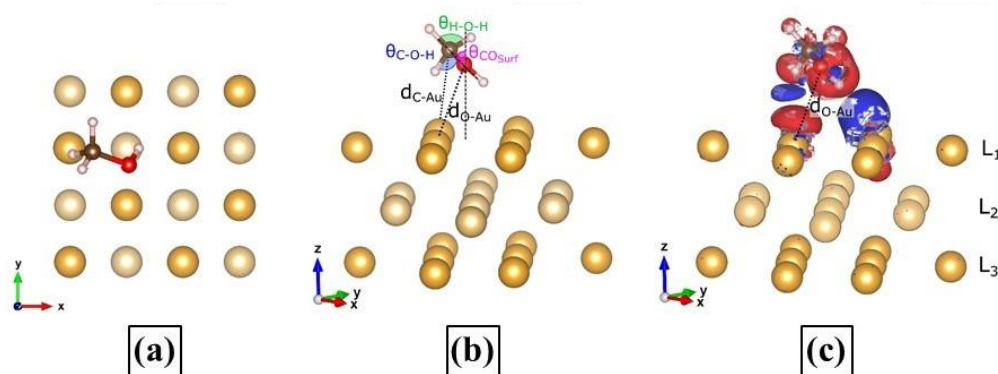
Fig. S6. Optimized structure for the MeOH molecule adsorbed on the Au(100) surface. (a) top and (b) side views. (c) Difference charge density, where the blue regions correspond to D>0, i.e. higher charge density due to adsorption, and red regions correspond to D<0, i.e. lower charge density due to adsorption. The Au atoms of the second layer L_2 are represented in light yellow.

The most stable adsorption occurs when the oxygen atom points towards the hollow site with an adsorption energy of -0.57 eV, see Fig. S6 and Table S3. In this arrangement, the C-O axis is tilted towards the surface forming an angle of θ_{COsurf} = 76.25° with respect to the Au surface normal. The distances from the O atom to the nearest Au atom (d_{O-Au}) and perpendicular to the Au surface (h_{O-sup}) are 0.315 and 0.280 nm, respectively, which are close to the sum of their anionic radii of 0.269 nm. We calculate that the adsorption of a MeOH molecule occurs via the donation of 0.029 electrons from the Au(100) surface to each MeOH molecule. Here, we report theoretical bond lengths that are in excellent agreement with experimental data (values in parentheses [10, 11]): 0.143 (0.1425) nm for the C-O bond, 0.097 (0.095) nm for the O-H bond, and 0.109 (0.109) nm for the C-H bond; the C-O-H and H-C-H angles are 107.4° (108.5°) and 109.7° (109.0°), respectively.

We found that the calculated binding energy for MeOH/Au(100) is 70% weaker than that for L-Cys/Au(100), so the L-Cys molecules should displace the MeOH ones and chemisorb directly onto the Au surface.

Table S3. E_{cys}^{ads} and d_{cys}^{ads} for systems shown in Figure S6. d_{cys}^{ads} is measured from the geometric centre of the MeOH molecule to the first Au atoms layer of the Au(100) surface. d_{O-Au} and d_{C-Au} are measured from the O and C atoms to the Au atom as shown in Figure S6.

System	E_{Met}^{ads} (eV)	d_{Met}^{ads} (nm)	d_{O-Au} (nm)	d_{C-Au} (nm)	θ_{HCO}
MeOH/Au	-0.57	0.298	0.315	0.332	107.04

C. Simulated STM images

C.1 *L-Cys monomer adsorbed on Au(100) surface*

Fig. S7 provides the results of the width of a L-Cys molecule adsorbed on a Au(100) surface obtained from the simulated STM image. According to STM experimental reports, each FL structure has an average width of $w_{SAM} = (2.0 \pm 0.2)$ nm. Theoretically, the width of a single L-Cys molecule adsorbed on gold is 0.82 nm, so each FL structure would have to be composed of at least two L-Cys molecules.
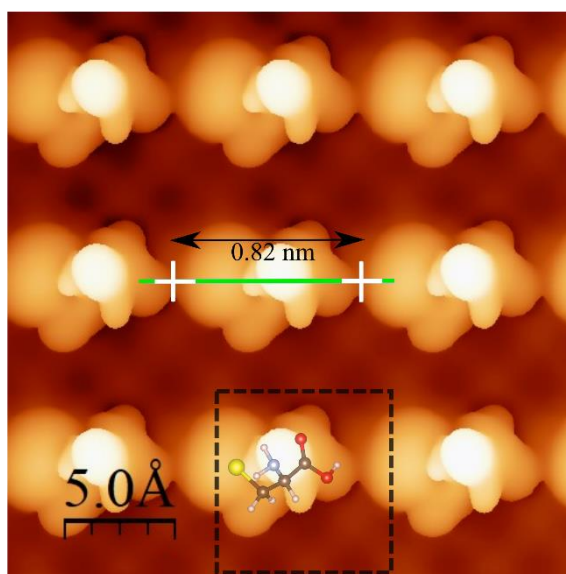
Fig. S7. Simulated STM image (2.5 nm × 2.5 nm) of L-Cys molecules adsorbed on a Au(100) surface. The image was simulated with a V_S = -0.80 V. The dashed line box corresponds to the simulated unit cell.

C.2 *L-Cys pairs adsorbed on Au(100) surface*

Fig. S8 shows the results of pairs of L-Cys molecules adsorbed on a Au(100) surface. From the data shown in Fig. S8(a) and S8(b), the simulated width of a pairs of L-Cys molecules adsorbed on a Au(100) surface, having a value of 1.93 nm, from which it is inferred that the width of the FL structures could be made up of two L-Cys molecules.
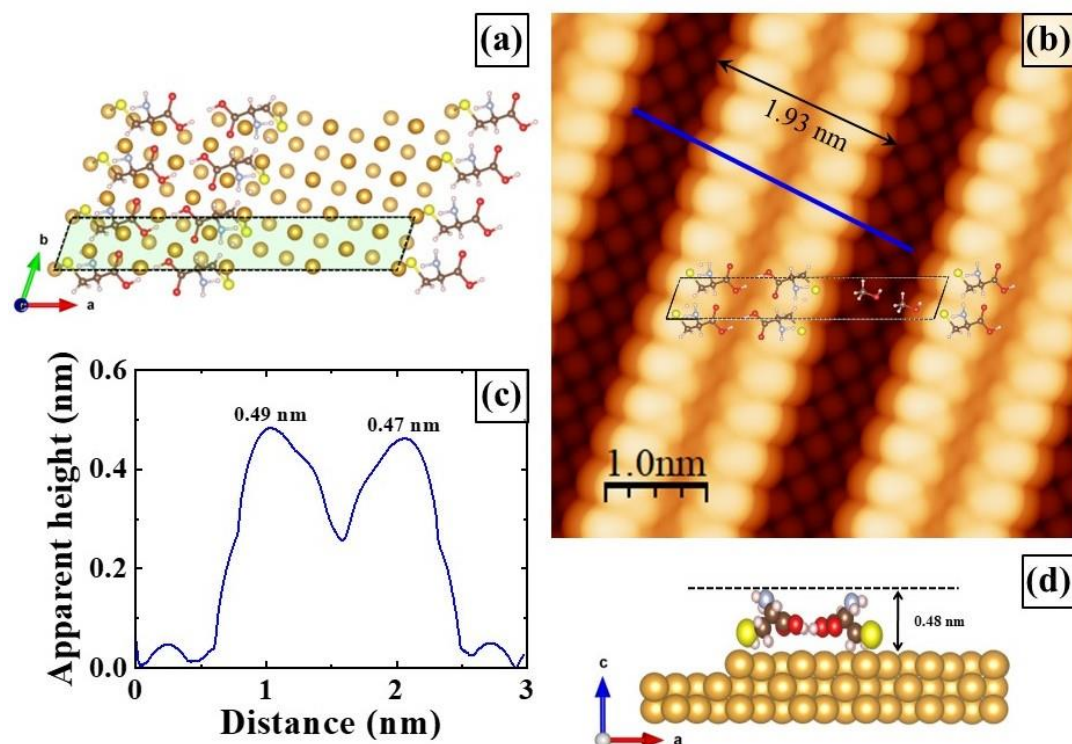
Fig. S8. L-Cys pairs of molecules adsorbed on a Au(100) surface, (a) supercell (top view), (b) simulated STM image (5.0 nm × 5.0 nm). The image was simulated with a V_s = -0.80 V, (c) profile of apparent heights acquired along the straight blue line depicted in image (b). (d) Side view of the supercell, the average height obtained from image (b) is 0.48 nm. The dashed line boxes in (a) and (b) correspond to the simulated unit cell.

REFERENCES

1. M. Kleinert, A. Cuesta, L. A. Kibler, and D. M. Kolb, "In-situ observation of an ordered sulfate adlayer on au(100) electrodes," Surf. Sci. **430**, L521(6) (1999).

2. O. Rodríguez de la Fuente, M. A. González, and J. M. Rojo, "Ion bombardment of recon- structed metal surfaces: from two-dimensional dislocation dipoles to vacancy pits," Phys. Rev. B **63**, 085420 (2001).

3. R. W. G. Wyckoff and J. Zemann, "Crystal structures," Acta Crystall. **18(1)**, 139 (1965).

4. N. Batina, A. S. Dakkouri, and D. Kolb, "The surface structure of flame-annealed Au(100) in aqueous solution: an STM study," J. Electroanal. Chem. **370**, 87 (1994).

5. L. J. Cristina, G. Ruano, R. Salvarezza, and J. Ferrón, "Thermal stability of self-assembled monolayers of n-hexanethiol on Au(111)-(1×1) and Au(001)-(1×1)," The J. Phys. Chem. C **121**, 27894 (2017).

6. D. Fedak and N. Gjostein, "On the anomalous surface structures of gold," Surf. Sci. **8**, 77(97) (1967).

7. D. Grumelli, L. J. Cristina, F. Lobo Maza, *et al.*, "Thiol adsorption on the Au(100)-

hex and Au(100)-(1×1) surfaces," The J. Phys. Chem. C **119 (25)**, 14248 (2015).

8. B. Pieczyrak, A. Trembulowicz, G. Antczak, and L. Jurczyszyn, "Nature of monovacancies on quasi-hexagonal structure of reconstructed Au(100) surface," Appl. Surf. Sci. **407**, 345 (2017).

9. M. V. Hove, R. Koestner, P. Stair, *et al.*, "The surface reconstructions of the (100) crystal faces of iridium, platinum and gold: I. experimental observations and possible structural models," Surf. Sci. **103**, 189 (1981).

10. M. N'dollo, P.S. Moussounda, T. Dintzer, B. M'Passi-Mabialaaand and F. Garin, "Density functional theory (DFT) investigation of the adsorption of the CH3OH/Au(100) system," Surf. Interface Analysis **45 (9)**, 1410 (2013).

11. D. Lide, *Handbook of Chemistry and Physic* (CRC Press, 1996).